

HIGH-RESOLUTION $H\alpha$ OBSERVATIONS OF PROPER MOTION IN NOAA 8668: EVIDENCE FOR FILAMENT MASS INJECTION BY CHROMOSPHERIC RECONNECTION

JONGCHUL CHAE, CARSTEN DENKER, TOM J. SPIROCK, HAIMIN WANG and
PHILIP R. GOODE

*Big Bear Solar Observatory, New Jersey Institute of Technology, 40386 North Shore Lane, Big Bear
City, CA 92314, U.S.A.*

(Received 29 March 2000; accepted 27 April 2000)

Abstract. There have been two different kinds of explanations for the source of cool material in prominences or filaments: coronal condensations from above and cool plasma injections from below. In this paper, we present observational results which support filament mass injection by chromospheric reconnection. The observations of an active filament in the active region NOAA 8668 were performed on 17 August 1999 at a wavelength of $H\alpha - 0.6 \text{ \AA}$ using the 65 cm vacuum reflector, a Zeiss $H\alpha$ birefringent filter, and a 12-bit SMD digital camera of Big Bear Solar Observatory. The best image was selected every 12 s for an hour based on a frame selection algorithm. All the images were then co-aligned and corrected for local distortion due to the seeing. The time-lapse movie of the data shows that the filament was undergoing ceaseless motion. The $H\alpha$ flow field has been determined as a function of time using local correlation tracking. Time-averaged flow patterns usually trace local magnetic field lines, as inferred from $H\alpha$ fibrils and line-of-sight magnetograms. An interesting finding is a transient flow field in a system of small $H\alpha$ loops, some of which merge into the filament. The flow is associated with a cancelling magnetic feature which is located at one end of the loop system. Initially a diverging flow with speeds below 10 km s^{-1} is visible at the flux cancellation site. The flow is soon directed along the loops and accelerated up to 40 km s^{-1} in a few minutes. Some part of the plasma flow then merges into and moves along the filament. This kind of transient flow takes place several times during the observations. Our results clearly demonstrate that reconnection in the photosphere and chromosphere is a likely way to supply cool material to a filament, as well as re-organizing the magnetic field configuration, and, hence, is important in the formation of filaments.

1. Introduction

The formation of prominences or filaments is one of the important unresolved problems in the study of the Sun. A successful model must explain the source of the cool material, as well as how the material is supported against gravity in a stable way. Basically, there have been two kinds of explanations for the mass supply to filaments: the condensation of coronal matter due to cooling, and the injection of cool plasma material from chromosphere or photosphere. Descriptions of early models of each kind were given by Tandberg-Hanssen (1974) and Malherbe (1989). More recent models which incorporate the idea of coronal condensation include Choe and Lee (1992, 1996a, and 1996b), Dahlburg, Antiochos, and Klimchuk (1998),



Solar Physics **195**: 333–346, 2000.

© 2000 Kluwer Academic Publishers. Printed in the Netherlands.



and Antiochos *et al.* (1999) while those which follow the idea of the cool material injection from below include Rust and Kumar (1994), Priest, van Ballegoijen, and Mackay (1996), and Litvinenko and Martin (1999).

This long-standing controversy may be mostly attributed to the difficulty of observationally discriminating between the two kinds of competing explanations. So far, the major supporting evidence for coronal condensation seems to be the existence of a cavity around a filament which could be interpreted as the original volume leading to coronal condensation. Furthermore, the matter which would be contained in the cavity region appears to be sufficient for the mass of a prominence (Engvold, 1989). But, further observations need to be made to verify the model of coronal condensation. Coronal condensation is a process of thermal evolution which involves shrinking motion. Therefore, verifying this model would require multi-wavelength observations with a good spatio-temporal resolution, which were virtually impossible until the recent experiments like SOHO and TRACE began to operate. The observational study of the thermal evolution of material in the coronal environment is still in the primitive stage, so we may have to wait for a while before we can observationally evaluate the model of coronal condensation.

Testing the model of cool material injection from below might be easier than doing that of coronal condensation. Since cool material injection would not involve drastic thermal evolution unlike coronal condensation, staying in only one or a few wavelengths of, for example, hydrogen lines will work for testing the model. Previous supporting evidence for cool material injection from below came from measurements of the vertical motion of filaments in $H\alpha$ and C IV which showed the existence of a mean upflow in filaments (Schmieder, 1989). But, until the nature of the observed mean upflow is fully understood, it is hard to confirm the model from such observations. For example, observationally verifying this model would require to show that the source region of such upflow is in the low atmosphere and the sink region is in filaments. It may also be necessary to clarify the physical cause of such upflow. In the present paper, we study proper motion around a filament in an active region using high resolution $H\alpha$ observations in the blue wing. Our results support that chromospheric, or photospheric reconnection is a likely way of filament mass injection as is proposed by Priest, van Ballegoijen, and Mackay (1996), and Litvinenko and Martin (1999).

2. Observations

We observed a filament in active region NOAA 8668 on 16 to 19 August 1999 at the Big Bear Solar Observatory (BBSO) during good seeing conditions. The daytime seeing characteristics of BBSO are discussed in Goode *et al.* (2000). Figure 1 shows a typical $H\alpha$ full-disk image which shows the position of the active region on the solar disk on 17 August. It also gives an enlarged view of the active region, which shows a C5.9 flare in progress. Full-disk $H\alpha$ data at the line center

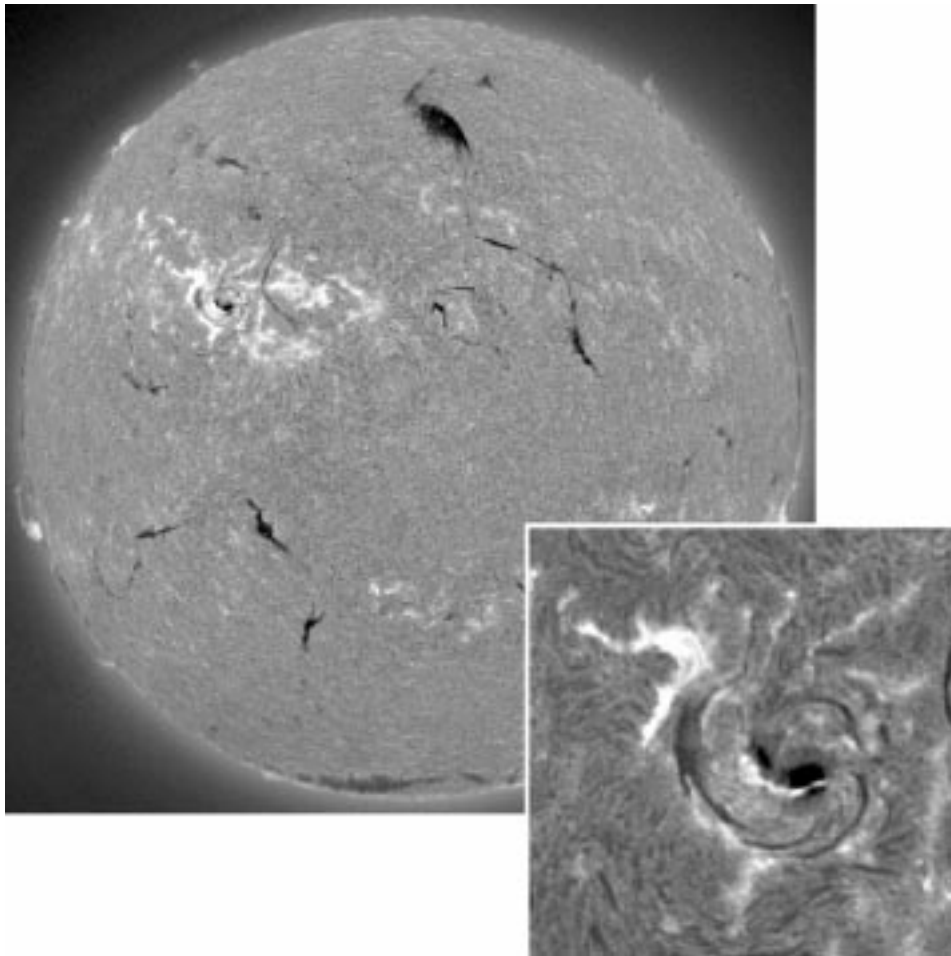


Figure 1. $H\alpha$ full-disk image obtained with the Singer telescope at 15:16 UT on 17 August 1999 during a C5.9 flare. The lower right panel shows the 250×250 arc sec² portion of the full-disk image depicting NOAA 8666 which has about the same field of view as high-resolution observations.

are routinely taken with the Singer $H\alpha$ full-disk telescope everyday at BBSO. A detailed description of the Singer $H\alpha$ full-disk telescope and the data processing of the $H\alpha$ filtergrams is given by Denker *et al.* (1999).

The active region was also observed with a high resolution mode in the $H\alpha$ line center using the OSL 12-bit digital camera attached to the 65 cm telescope. Figure 2 shows some of the high-resolution $H\alpha$ center line images taken by this camera. The OSL camera has 512×512 pixels after 2×2 pixel binning. During these days, the filament changed its shape a lot, growing longer and darker. Obviously the filament was under formation and grew to be of the inverse *S*-shape. Filaments and coronal loops of either *S*- or inverse *S*-shape are called sigmoids (Rust and Kumar, 1996). Sigmoids often produce flares and coronal mass ejections which may

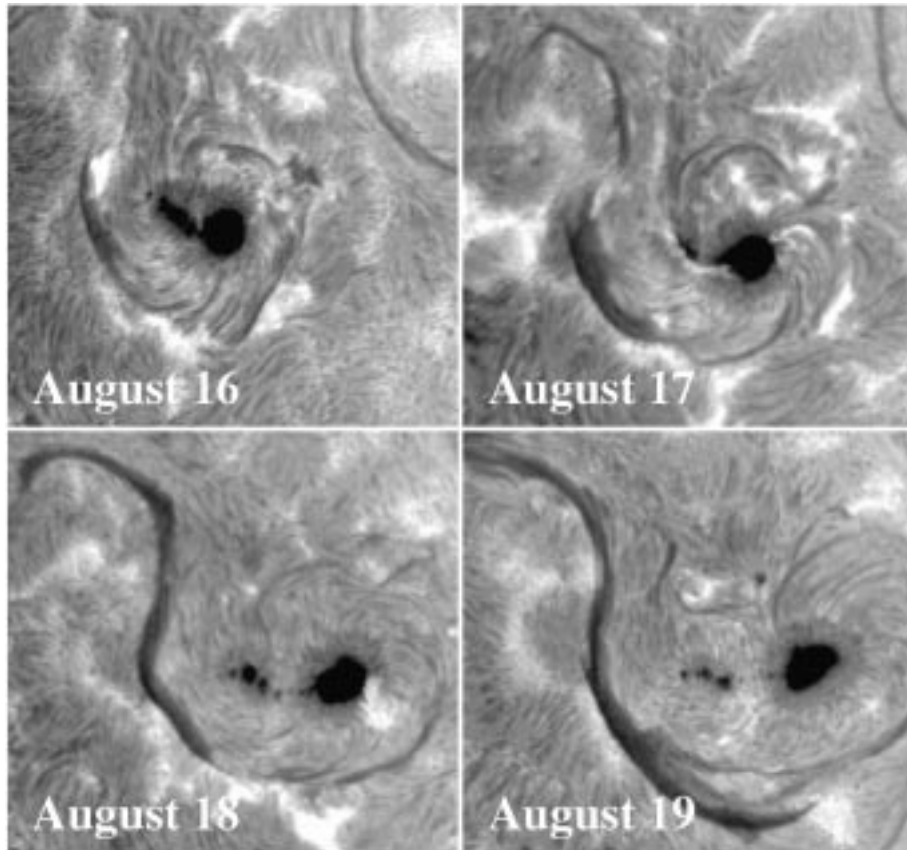


Figure 2. The evolution of the filament in the active region as observed in the $H\alpha$ center line. The images were taken by the OSL digital camera attached to the BBSO 65 cm telescope.

affect space weather (Canfield, Hudson, and McKenzie, 1999). The continuously changing morphology and contrast seen in the figure suggests that the formation of this sigmoid filament may have involved two kinds of physical processes: magnetic topology change and mass supply. We investigate these processes by studying $H\alpha$ proper motion.

On 17 August 1999, we used a faster digital camera in place of the OSL camera for about an hour. The camera used is the Silicon Mountain Design 1M15 frame transfer CCD camera which was recently acquired by BBSO. It has 512×512 pixels after 2×2 binning. The image scale is $0.45 \text{ arc sec pixel}^{-1}$, so the camera covers a field of view of about $230 \times 230 \text{ arc sec}$. Making use of the high frame rate of 30 s^{-1} , we applied frame selection to obtain high quality images. The exposure time was taken to be 8 ms which is sufficiently short to ‘freeze’ the atmospheric turbulence. A sequence of 200 filtergrams were stored in the RAM of the camera control computer for 7 s and only the image with the highest rms contrast was saved to hard disk. We repeated this process every 12 s and obtained a total of

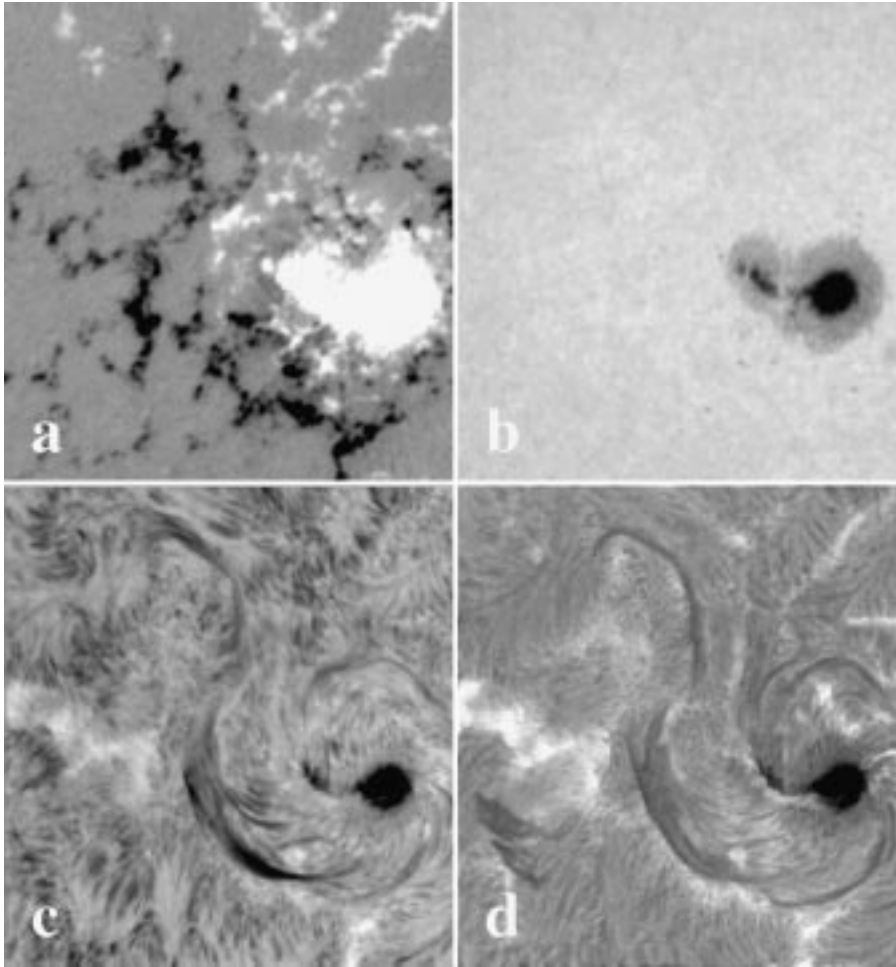


Figure 3. (a) Videomagnetogram and (b) filtergram of NOAA 8666 taken at the wing of the photospheric Ca I line at 6103 \AA with the 25 cm vacuum refractor at 15:57 UT on 17 August 1999. (c) $H\alpha - 0.6 \text{ \AA}$ (17:16 UT) filtergram taken with the SMD camera on the 65 cm vacuum refractor. (d) $H\alpha$ centerline filtergram (17:47 UT) taken with the OSL camera. The field of view is $200 \times 220 \text{ arc sec}^2$.

240 selected filtergrams during the time period from 16:27 UT to 17:16 UT. The wavelength of these $H\alpha$ observations was tuned to $H\alpha - 0.6 \text{ \AA}$. We have chosen the blue wing of the line since we are mainly interested in blue-shifted features, which may be visible when mass is injected to the filament from below.

Figure 3 shows a co-aligned $H\alpha$ offband image of the active region taken at -0.6 \AA by the new SMD digital camera, and a $H\alpha$ centerline image of the same area taken by the OSL camera. The figure also shows a high resolution line-of-sight magnetogram, and the white-light image of the active region. The magnetogram was obtained by the videomagnetograph system on the 25 cm vacuum refractor. A

description of the videomagnetograph system and its calibration is given by Varsik (1995). We obtained about 120 sets of videomagnetograms at a cadence of about 1 min from 15:21 UT to 17:54 UT.

3. Determination of H α Proper Motion

To determine the proper motion of H α features, we apply the technique of local correlation tracking (LCT) which was originally applied to photospheric structures such as granulation, sunspots, and pores (e.g., November and Simon, 1988). To minimize the effects of the Earth's turbulent atmosphere (seeing), we first aligned the images rigidly and subsequently destretched the images with respect to the mean image obtained by averaging over all the 240 frames. The advantage of using only one reference image for destretching is that there is no worry about relative displacements of different reference images which may exist in case more than one reference images are used. In addition, an iterative maximum entropy algorithm (Chae *et al.*, 1998), has been applied to the images to enhance their contrast and to equalize the power spectral density of the images.

Measuring flow fields of chromospheric structures, as seen in the H α line, by means of LCT is somewhat different from measuring photospheric flow fields in a couple of ways. First of all, the contrast of chromospheric structures seen through a narrow-band filter tuned to the line wings of H α may be strongly influenced by Doppler shifts (Yi and Molowny-Horas, 1995). These contrast fluctuations are picked up by the LCT algorithm, and cause a cross-talk between horizontal proper motions and Doppler shifts. This possibility should be kept in mind in interpreting the results. An advantage in measuring chromospheric flow fields is that the typical velocity in the chromosphere (which is of the order of 10 km s^{-1}) is much larger than those in the photosphere (which is of the order of 1 km s^{-1}) and, hence, is less subject to image distortion due to the seeing. Nevertheless, the effect of the seeing is not negligible even in determining chromospheric flow fields.

An apodizing window function with a shape of a Gaussian was chosen for computation of the displacement vector at each spatial point. An optimal value of the FWHM of the apodizing function depends on the size of the smallest features seen in the data – which is practically limited by the seeing – and by the noise level. We varied the FWHM value of the apodizing function, and examined the resulting speeds of the velocity structures and found that the flow velocity increased only by 10% when the FWHM was decreased from 3.6 arc sec to 2 arc sec. This seems to suggest that the flow field, which possibly is confined to small-scale structures, is largely uni-directional over several arcseconds, i.e., within areas equal to or larger than the apodizing window. Decreasing the FWHM of the apodizing window increases the random velocity components caused by noise. We have therefore safely chosen FWHM = 3.6 arc sec.

For determining each velocity field at an instant, we have to pick two consecutive images taken apart in time. We select the time interval of 24 s, which is twice the time resolution. This choice appears reasonable, since the corresponding spatial shifts (which range from 240 to 960 km with flow speeds between 10 and 40 km s⁻¹) are big enough to be determined from LCT (i.e., bigger than a few tenths of the pixel size, 325 km), and are small enough not to escape from the apodizing window with the FWHM of 2500 km. We take averages of measured flow fields over the time interval of 96 s to minimize the effect of image distortion due to the seeing. A value much smaller than this makes distortion-induced velocity fields dominate over true velocity fields, and a bigger value excessively suppresses intrinsic velocity fields.

We would like to mention that LCT equally well traces both dark absorption features and bright emission features. This was easily checked by comparing velocity fields determined from negative images – in which dark absorption features appear bright and *vice versa* – with the ones determined from the original images. We could not find any difference between the two. The reason is simple. What matters in LCT is the magnitude of contrast of the feature as is measured with respect to the local average, and not the sign of contrast. This justifies our application of LCT to H α data in which prominent features mostly appear in absorption.

4. Results

4.1. GENERAL CHARACTERISTICS OF PROPER MOTION SEEN IN H α BLUE WING

On the CD-ROM we provide an MPEG movie of H α -0.6 Å data which covers a period of approximately 50 min. Note that, to save computer memory and speed required for display, only a quarter of all the images taken have been used for this movie. This limits the time resolution of the constructed movie to be about 50 s, much poorer than that of the real observation of 12 s. Nevertheless, the movie is good enough to demonstrate that the chromosphere seen in the H α blue wing is undergoing ceaseless and various motions everywhere in this active region. Since the observations are made in the blue wing of H α , we may be looking at much more upward moving features than downward moving features. Thus proper motions along fibrils which are the most commonly seen in the movie are likely to mostly represent the transverse components of rising motion along inclined fibrils. In addition, we see a surge-like small H α jet near the sunspots, an outward-propagating penumbral wave in the big sunspot, the flows along the small H α loops near the lower half part of the filament, the eruptions of the upper half part of the filament, and H α plasma streamings presumably along coronal loops, transiently visible around 16:50 UT at the left portion of the movie.

In Figure 4, we show the average flow map derived from all the 240 H α -0.6 Å filtergrams. The average velocity is 4.4 ± 2.8 km s⁻¹ and the maximum velocity is

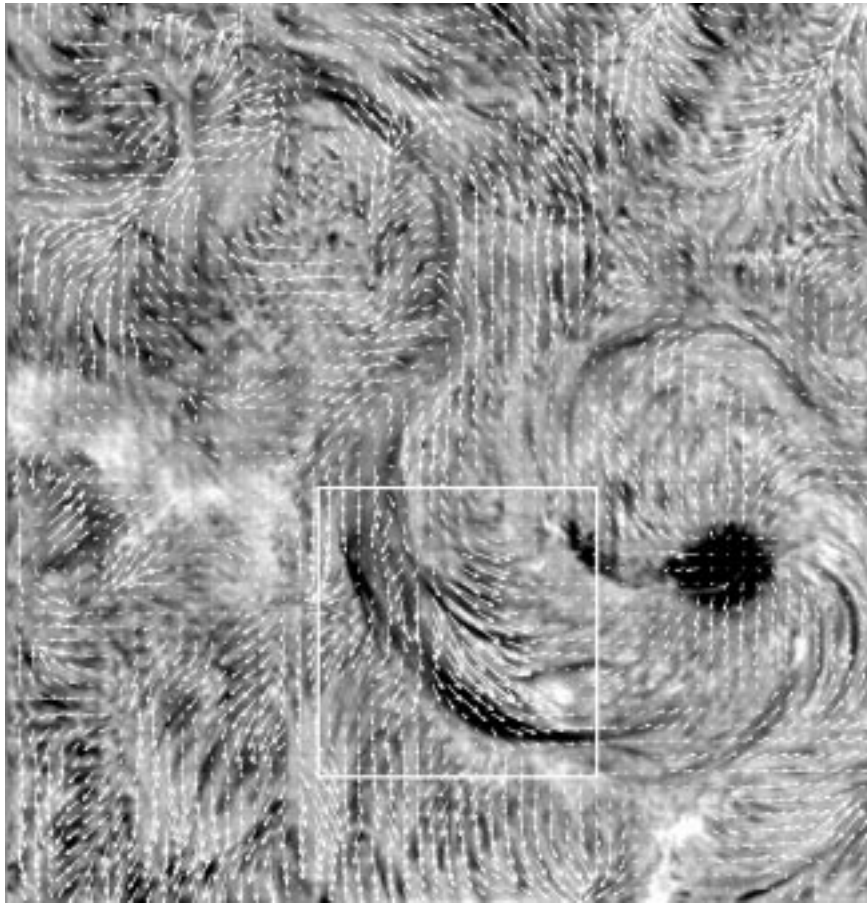


Figure 4. Average flow map of $H\alpha$ line wing filtergrams determined from all the 240 filtergrams. The field of view is 210×218 arc sec².

20.6 km s^{-1} . The time averaging removes most of image distortion due to seeing and the short-lived transient flows, leaving only persistent flows which are either steady or recurring many times at the same places. An important general characteristic of $H\alpha$ proper motion is that the time-averaged flow fields appear as plasma streamings which usually well trace local magnetic field lines. This is clear from the fact that the velocity vectors are well aligned with $H\alpha$ fibrils and fine threads which have traditionally been known as magnetic field line proxies (e.g., Foukal, 1971). This characteristic is also obvious in the proper motions around the sunspot which are radially directed out of the sunspot center. This kind of characteristic in $H\alpha$ proper motion has been used to infer the magnetic field structures in complicated quiescent filaments based on the observations of counter-streaming flows (Zirker, Engvold, and Martin, 1998; Martin, 1998).

A persistent pattern of large proper motion is found in the region indicated by the white box in Figure 4. This region shows a part of the filament and a set of small $H\alpha$ loops. Comparison of the $H\alpha$ blue wing and centerline images (see Figure 3) shows that the $H\alpha$ loops are more prominent in the blue wing image than in the centerline image. This implies that the plasma in these loops is blue-shifted, and, hence, is rising upwards. This region is particularly interesting to us since it provides evidence for cool mass injection to the filament. In the following, we will examine in detail the characteristics of proper motion and magnetic field change in this region.

4.2. A TRANSIENT $H\alpha$ UPFLOW EVENT

Figure 5 shows the time variation of the $H\alpha-0.6 \text{ \AA}$ proper motion in the region of interest as well as the image itself. Initially at 16:30 UT, there are no significant velocity fields, but a set of $H\alpha$ loops is clearly visible in the field of view. At 16:33 UT, diverging velocity fields are seen at the one side of the loop system, which is indicated by the white small box. We believe that this position is a mass source region from which material begins to be accelerated. The velocity is smaller than 10 km s^{-1} near the center of the diverging flow area, but reaches up to 20 km s^{-1} at the outer part of the area. In a few minutes, as seen at the times of 16:36 UT and later, the flow pattern changes into a more or less uni-directional one along the loops.

A careful comparison of the velocity fields at 16:33 UT and later reveals that the position of the maximum velocity itself moves in the same direction as the velocity vectors indicate. It takes about 6 minutes for the position to move a distance of 13 000 km, which indicates that the maximum position is moving at a speed of about 35 km s^{-1} . This value is a little larger than, but is not incompatible with the value of the maximum velocity, ranging from 25 to 40 km s^{-1} , which has been determined from LCT. Thus, the determined velocity fields must represent real transient plasma motions.

The flows as a whole clearly define streamlines which are very likely to follow local magnetic field lines. A very interesting fact is that some of streamlines merge into the filament as seen at 16:36 and later. At these times, we find velocity fields even inside the filament, which follow the filament axial direction. Figure 5 also shows the divergence map of the mean flow field determined by averaging over the 12 min period. It is clear from the divergence map that there is a source in the region indicated by the small white box and there is a sink in the filament body. Therefore, it appears that cool plasma material is being injected to the filament along the magnetic field lines which connects through the source region and the filament body.

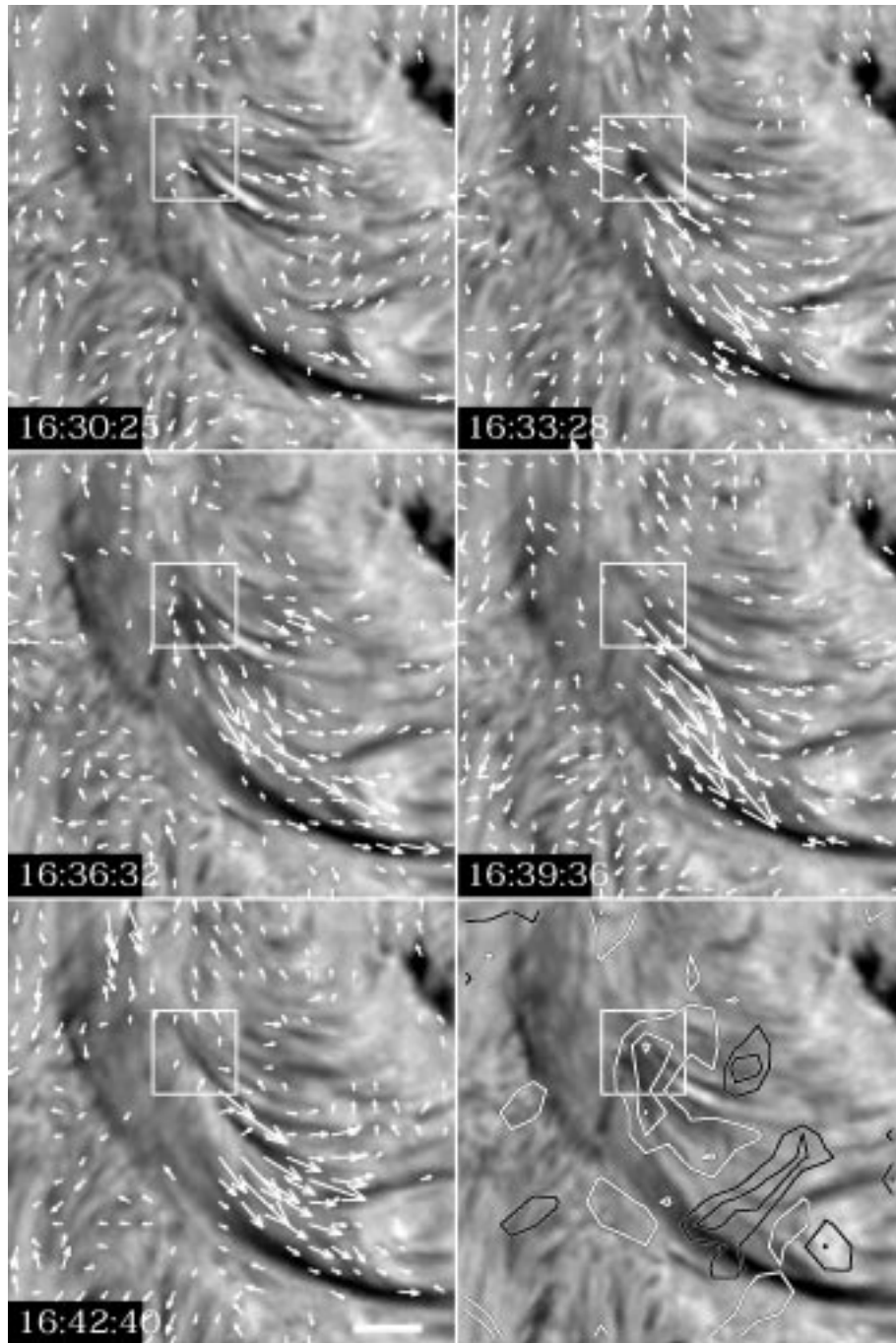


Figure 5. The time variation of 100 s-averaged $H\alpha-0.6 \text{ \AA}$ flow field (the first five panels), and the divergence map of the 12 min-averaged flow field (the last panel). The length of the bar in the lower left corner panel corresponds to flow speed of 30 km s^{-1} . Velocity arrows with speeds smaller than 3 km s^{-1} were suppressed for clarity. The divergence contours are $\pm 5, 10,$ and $15 \text{ km s}^{-1} \text{ Mm}^{-1}$ with the white ones representing the positive values (source) and the black ones, the negative values (sink). The small white box represents the location of the cancelling magnetic feature. The field of view is $67 \times 67 \text{ arc sec}^2$.

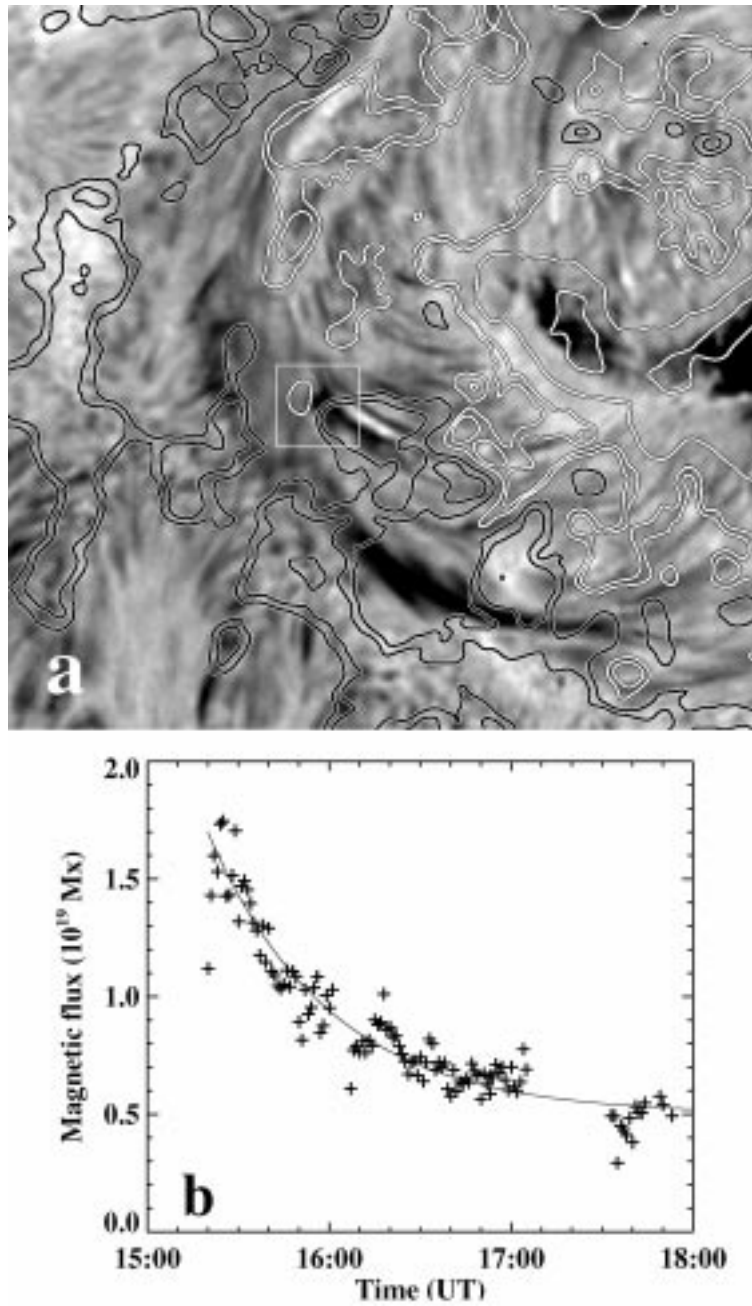


Figure 6. (a) Magnetic configuration of the sub-region showing the filament and a set of H α loops. Superposed are contours of the apparent flux density levels at ± 50 , 100, 400, and 800 gauss. The cancelling magnetic feature is indicated by the small white box. (b) Time variation of magnetic flux of the positive flux concentration in the cancelling magnetic feature. The solid curve is an exponential function fit to the observations.

4.3. MAGNETIC FIELD CHANGE

We examine the configuration of magnetic fields in the active region and a possible magnetic field change associated with the H α flow event. As seen in Figure 3, the filament is near the polarity inversion line between the leading polarity positive flux region and the trailing negative flux region. Figure 6a shows the detailed magnetic map superposed on the H α image of the region of interest. The part of the filament shown in this appears to be a small distance away from the polarity inversion line. This may be partly attributed to the perspective view of the filament in the line-of-sight direction which is highly inclined to the vertical on the solar surface. Nevertheless, the map clearly shows that the northern ends of the filament threads are rooted in the negative flux regions, whereas the southern ends are rooted in the positive flux regions. This means that the axial field of the filament is rightward when seen by an observer at the positive flux region. Therefore, the filament is dextral.

From Figure 6a, we find a converging magnetic bipole at the location of the diverging H α flow as indicated by the small white box. Converging magnetic bipoles usually correspond to cancelling magnetic features. The time sequence of BBSO magnetograms clearly shows that the bipole is a cancelling magnetic feature. The cancelling magnetic feature lies near the polarity inversion line of the global flux distribution. Figure 6b shows the positive magnetic flux in the cancelling magnetic feature as a function of time. It is interesting that the time variation of the flux is fairly well described by an exponentially decreasing function of the form

$$F = A \exp[-(t - t_0)/\tau] + B \quad (1)$$

with the values of $A = 1.2 \times 10^{19}$ Mx, $B = 0.5 \times 10^{19}$ Mx, and $\tau = 40$ min. Since the fluxes of other magnetic features remain more or less constant with time unlike this feature, we see that this exponential decrease is not due to the degradation of seeing, but represents an intrinsic change. The implied flux loss rate during the observation is 2 to 3×10^{15} Mx s $^{-1}$, which is of the same order of magnitude as the rate reported for the flux cancellation associated with small H α surges in active region NOAA 8264 (Chae *et al.*, 1999).

The time variation of the flux shown in Figure 6 indicates that the flux was cancelling before the start of the H α flow event. Moreover, the flux cancelling timescale is longer than that of the H α flow event. This may suggest that more than one H α event was occurring during the flux cancellation. This possibility is supported by our finding from the whole set of data that there are a couple of similar H α events in addition to the one presented in Figure 5.

5. Discussion

Our high-resolution $H\alpha$ and magnetograph observations have produced results which support the idea of filament mass injection driven by chromospheric reconnection as inferred from the previous observations (e.g., Martin, 1998) and theoretically modeled by Priest, van Ballegoijen, and Mackay (1996) and Litvinenko and Martin (1999). Most of all, we have found well-defined cool plasma streamings which connect the source region and the filament body. Since the flow is upward, the source region should be located much lower than the filament, possibly in the chromosphere. Secondly, the source region has a diverging flow pattern when the cool plasma begins to be accelerated. This pattern is exactly the one expected near the magnetic reconnection point. Since the reconnection outflow is driven mostly by the tension force of the destretching reconnected field lines, the flow tends to diverge from the reconnection point until the reconnected field lines are fully destretched (see Figure 7 of Priest, van Ballegoijen, and Mackay, 1996).

We also see a cancelling magnetic feature at the very location of the $H\alpha$ flow source. This is evidence that reconnection (e.g., van Ballegoijen and Martens, 1989) drives the $H\alpha$ flow. Furthermore, the reconnection must be occurring below the level which we are looking in $H\alpha$, since the dominant $H\alpha$ motion is upward at the location of reconnection. So the reconnection may be occurring in the low chromosphere, or in the photosphere, or even below the photosphere. There is no way of telling from our observation which level is the most probable. Nevertheless, it is likely that this reconnection is totally different from coronal reconnection which is known to be responsible for flares, since we do not see any evidence for hot plasma material associated with the observed reconnection. Thus, in contrast to coronal reconnection, we may call it chromospheric reconnection, even if we do not know the specific atmospheric level of the reconnection event. Some theoretical works favor the temperature minimum level for this kind of reconnection, different from coronal reconnection, to occur since the classical electric conductivity is low enough (Chae, 1999; Litvinenko, 1999; Sturrock, 1999).

Based on our results, we can understand why the existence of cancelling magnetic features is essential in the formation of filaments, as is well known from previous observations (for review, see Martin, 1998). The reason is that chromospheric reconnection is important not only in re-configuring magnetic fields required to support filaments, but also in filling filaments with cool material.

Acknowledgements

We would like to thank Dr. Louis Strous for providing the LCT routines and Dr. Jiong Qiu for careful reading of the manuscript. We are indebted to the referee's comments for the improvement of the paper. J. Chae is grateful to God who gave him the joy and ability to investigate the topic treated in this paper. This work was

supported by NSF under grant ATM 97-14796 and INT-98-16267, by ONR under grant N00014-97-1-1037, and by NASA under grant NAG5-4919, NAG5-7350 and NAG5-7837.

References

- Antiochos, S. K., Macneice, P. J., Spicer, D. S., and Klimchuk, J. A.: 1999, *Astrophys. J.* **512**, 985.
- Canfield, R. C., Hudson, H. S., and McKenzie, D. E.: 1999, *Geophys. Res. Lett.* **26**, 627.
- Chae, J.: 1999, in *19th NSO/SP International Workshop on High Resolution Solar Physics: Theory, Observations, and Techniques, Asp Conf. Ser.* **183**, 375.
- Chae, J., Yun, H. S., Sakurai, T., and Ichimoto, K.: 1998, *Solar Phys.* **183**, 245.
- Chae, J., Qiu, J., Wang, H., and Goode, P. R.: 1999, *Astrophys. J.* **513**, L75.
- Choe, G. S. and Lee, L. C.: 1992, *Solar Phys.* **138**, 291.
- Choe, G. S. and Lee, L. C.: 1996a, *Astrophys. J.* **472**, 360.
- Choe, G. S. and Lee, L. C.: 1996b, *Astrophys. J.* **472**, 372.
- Dahlburg, R. B., Antiochos, S. K., and Klimchuk, J. A.: 1998, *Astrophys. J.* **495**, 485.
- Denker, C., Johannesson, A., Marquette, W. H., Goode, P. R., Wang, H., and Zirin, H.: 1999, *Solar Phys.* **184**, 87.
- Engvold, O.: 1989, *Dynamics and Structure of Quiescent Solar Prominences*, Kluwer Academic Publishers, Dordrecht, p. 47.
- Foukal, P.: 1971, *Solar Phys.* **19**, 59.
- Goode, P. R., Wang, H., Marquette, W. H., and Denker, C.: 2000, *Solar Phys.*, **195**, 421 (this issue).
- Litvinenko, Y.: 1999, *Astrophys. J.* **515**, 435.
- Litvinenko, Y. and Martin S. F.: 1999, *Solar Phys.* **190**, 45.
- Malherbe, J.-M.: 1989, *Dynamics and Structure of Quiescent Solar Prominences*, Kluwer Academic Publishers, Dordrecht, p. 115.
- Martin, S. F.: 1998, *Solar Phys.* **182**, 107.
- November, L. J. and Simon, G. W.: 1988, *Astrophys. J.* **333**, 427.
- Priest, E. R., van Ballegoijen, A. A., and Mackay D. H.: 1996, *Astrophys. J.* **460**, 530.
- Rust, D. M. and Kumar, A.: 1994, *Solar Phys.* **155**, 69.
- Rust, D. M. and Kumar, A.: 1996, *Astrophys. J.* **464**, L199.
- Schmieder, B.: 1989, *Dynamics and Structure of Quiescent Solar Prominences*, Kluwer Academic Publishers, Dordrecht, p. 15.
- Sturrock, P. A.: 1999, *Astrophys. J.* **521**, 451.
- Tandberg-Hanssen, E.: 1974, *Solar Prominences*, D. Reidel Publ., Dordrecht, Holland.
- Varsik, J. R.: 1995, *Solar Phys.* **161**, 207.
- van Ballegoijen, A. A. and Martens, P. C. H.: 1989, *Astrophys. J.* **343**, 971.
- Yi, Z. and Molowny-Horas, R.: 1995, *Astron. Astrophys.* **295**, 199.
- Zirker, J. B., Engvold, O., and Martin, S. F.: 1998, *Nature* **396**, 440.